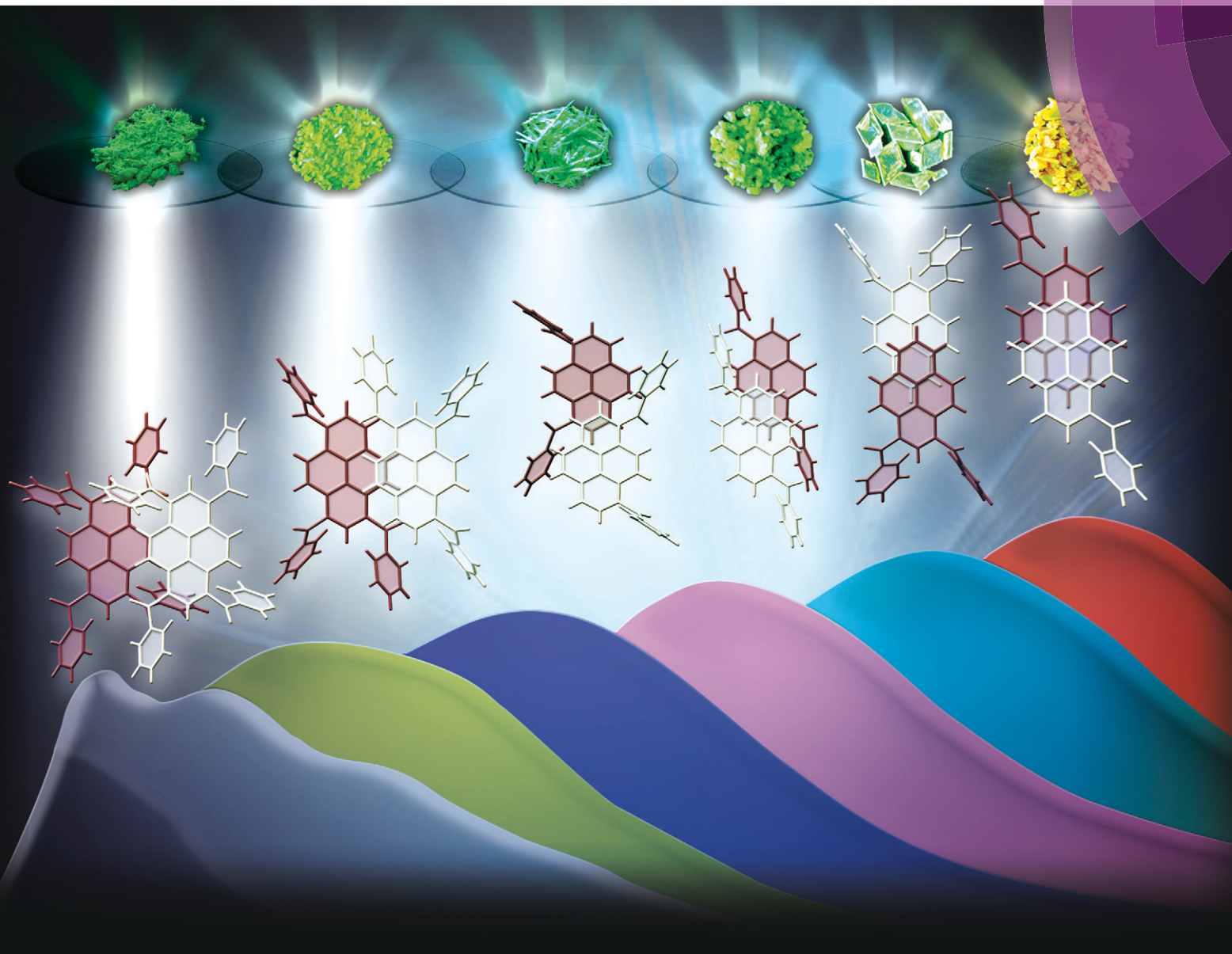


# CrystEngComm

[www.rsc.org/crystengcomm](http://www.rsc.org/crystengcomm)



**PAPER**

Mahesh Hariharan *et al.*

Crystallization induced green-yellow-orange emitters based on benzopyrenes

**175** YEARS



Cite this: *CrystEngComm*, 2016, 18, 5089

Received 17th March 2016,  
Accepted 26th April 2016

DOI: 10.1039/c6ce00610h

www.rsc.org/crystengcomm

# Crystallization induced green-yellow-orange emitters based on benzoylpyrenes†

Shinaj K. Rajagopal, V. Sivaranjana Reddy and Mahesh Hariharan\*

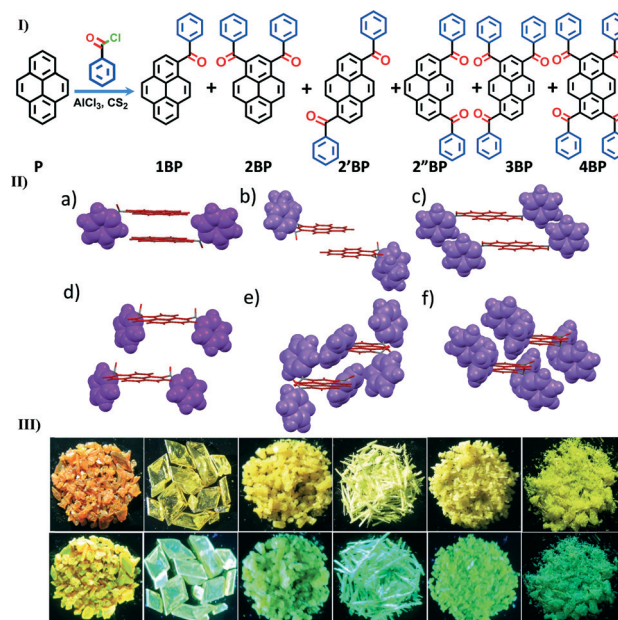
We report the synthesis, X-ray structures and photophysical properties of a few benzoylpyrene (BP) derivatives. Steric hindrance due to incremental benzoyl groups causes a systematic reduction in the orbital overlap ( $\pi$ - $\pi$ ) between vicinal pyrene units affording green-yellow-orange solid-state emitters. Crystallization induced emission could arise from: i) electronic (dipolar/excitonic) interactions, ii) arrested bond rotations, and/or iii) lack of solvation in crystalline 1-4BP ( $\Phi_{\text{Fl}} \sim 2$ –26%) when compared to that in solution ( $\Phi_{\text{Fl}} \leq 1\%$ ). Our earlier effort [*Chem. Commun.* 2014, 50, 8644] on progressive acylation, in contrast to benzylation, results in a gradual increase in the  $\pi$ - $\pi$  overlap between vicinal pyrenes.

## 1. Introduction

Pyrene is considered as fruit fly of photochemists by virtue of its versatile photophysical properties that can be exploited in fundamental and applied research.<sup>1</sup> Since the discovery of pyrene in 1837,<sup>2</sup> this unique chromophore has been well-exploited for diverse applications in biology and materials science owing to its inherent photochemical stability. Crystalline pyrene based blue organic light emitting devices (OLEDs) suffer from strong excimer contributions.<sup>3</sup> Disruption of nearest neighbour interactions in crystalline pyrene is expected to enhance the performance of OLEDs.<sup>4</sup> A variety of chemical<sup>5</sup> and physical approaches<sup>6</sup> have been utilized to regulate pyrene-pyrene interactions. Physical methods to tune these interactions<sup>7</sup> involve mechanical grinding,<sup>8</sup> sublimation<sup>9</sup> or solvent/co-crystallization.<sup>6a</sup> Chemical methods<sup>10</sup> employ steric effects imparted by bulky groups that can be conveniently functionalized through electrophilic substitution reactions. Most of such attempts have led to the conversion of dimeric to monomeric pyrene, resulting in a shift from “deep-blue” to “sky-blue” solid state emission.<sup>11</sup> Yet the synthesis and structure-property correlation of pyrene based non-blue solid state emitters has received less attention.

Recently, we utilised interchromophoric interactions of pyrene to understand the distribution of parallel vs. antiparallel G-quadruplex conformations in aqueous and non-aqueous media.<sup>12</sup> Efforts to tune the interchromophoric interactions in molecular crystals using  $\pi$ - $\pi$ ,<sup>13</sup> C-H $\cdots$  $\pi$ ,<sup>14</sup> C-H $\cdots$ O<sup>15</sup> and C-H $\cdots$ H-C<sup>16</sup> contacts for favourable photo-

physical properties allowed us to employ the combination of steric and conjugation effects of benzoyl units of pyrene based systems. In our earlier effort,<sup>13a</sup> progressive acylation of pyrene resulted in a remarkable decrease in the interplanar angle between two neighbouring units causing significant red-shift in the solid-state fluorescence. The significant dimension of the benzoyl unit (129.4 Å<sup>3</sup>)<sup>17</sup> as compared to pyrene (237.5 Å<sup>3</sup>) could potentially perturb strong  $\pi$ - $\pi$  interactions ( $-13.8$  kcal mol<sup>-1</sup>)<sup>18</sup> between the



**Scheme 1** Row I: molecular structures of 1-4BP; row II: close packing arrangements in the crystals a) 1BP; b) 2BP; c) 2'BP; d) 2''BP; e) 3BP and f) 4BP; row III: photographic images of crystals in daylight (above) and under UV illumination (below).

School of Chemistry, Indian Institute of Science Education and Research  
Thiruvananthapuram, CET Campus, Sreekaryam, Thiruvananthapuram, Kerala,  
India 695016. E-mail: mahesh@iisertvm.ac.in

† Electronic supplementary information (ESI) available: <sup>1</sup>H NMR and <sup>13</sup>C NMR spectra of BP derivatives, summary of crystal structures and refinement details of 1-4BP. CCDC 1440151-1440156. For ESI and crystallographic data in CIF or other electronic format see DOI: 10.1039/c6ce00610h

nearest pyrene units (center-to-center distance of 3.53 Å; Fig. S1; ESI<sup>†</sup>). In addition, the conjugation arising from incremental benzoyl units progressively influences the HOMO–LUMO gap that could result in bathochromic shift in electronic absorption and emission properties. We herein report simple Friedel–Crafts benzoylation of pyrene (Scheme 1, row I) that results in the formation of green-yellow-orange luminescent crystals. In contrast to the acylation of pyrene,<sup>13a</sup> progressive benzoylation of pyrene resulted in a significant decrease in the  $\pi$ – $\pi$  interactions causing systematic blue-shift in the emitted light in the crystalline state. Crystallization induced emission (CIE) possessing precise emission colour tunability in benzoylpyrene derivatives indicates the possibility for novel light emitting devices.

## 2. Experimental

### 2.1 Materials and methods

Reactions were carried out in oven-dried glassware prior to use and, wherever necessary, were performed under dry nitrogen in dried, anhydrous solvents using standard gastight syringes, cannulae, and septa. Solvents were dried and distilled by standard procedures. Flash column chromatography was performed using silica gel of 200–400 mesh employing a solvent polarity correlated with the TLC mobility observed for the substance of interest. Yields refer to chromatographically and spectroscopically homogeneous substances. High Resolution Mass Spectra (HRMS) were recorded on an Agilent 6538 Ultra High Definition (UHD) Accurate-Mass Q-TOF-LC/MS system using either atmospheric pressure chemical ionization (APCI) or electrospray ionization (ESI) mode. <sup>1</sup>H and <sup>13</sup>C NMR spectra were measured on a 500 MHz Bruker advanced DPX spectrometer. The internal standard used for <sup>1</sup>H and <sup>13</sup>C NMR is 1,1,1,1-tetramethyl silane (TMS). All the elemental analyses were performed on an Elementar Vario MICRO Cube analyzer. All values recorded in elemental analyses are given in percentages. The reference standard used for elemental analysis is 4-aminobenzenesulphonic acid (sulphanilic acid).

### 2.2 Synthetic procedure

Preparation of benzoylpyrene (1–4BP) derivatives:<sup>19</sup> pyrene (10 g; 0.049 mol) dissolved in CS<sub>2</sub> (yellow solution, 250 mL) was maintained at ambient temperature and subsequently anhydrous AlCl<sub>3</sub> was added. Benzoyl chloride (27.80 g; 0.198 mol) was then slowly syringed to the suspension. Subsequently, hydrogen chloride was liberated. After 3 hours, the mixture was added slowly to a vigorously stirred mixture of ice and concentrated HCl. The resulting suspension was filtered, vacuum dried and purified through column chromatography (silica gel) to give benzoylpyrene (1–4BP) derivatives.

1BP (yield = 5.1%) M.p. 102–105 °C. <sup>1</sup>H NMR [500 MHz, DMSO(*d*<sub>6</sub>),  $\delta$ ]: 8.40 (m, 4H), 8.43 (q, *J* = 9.66 Hz, 2H), 8.17 (m, 3H), 7.82 (d, *J* = 7.7 Hz, 2H), 7.73 (t, *J* = 7.2 Hz, 1H), 7.58 (d, *J* = 7.8 Hz, 2H). <sup>13</sup>C NMR [125 MHz, DMSO(*d*<sub>6</sub>),  $\delta$ ]: 197.56, 138.0, 133.60, 132.82, 132.46, 130.70, 130.08, 129.07, 128.90, 128.83, 128.66, 127.25, 126.83, 126.68, 126.35, 126.04, 124.20,

124.10, 123.84, 123.55. IR (KBr, cm<sup>-1</sup>): 3037, 1651, 1595, 1506, 1446. Elemental analysis: calcd. value for C<sub>23</sub>H<sub>14</sub>O: 90.17% C, 4.61% H; found: 90.31% C, 4.56% H. HRMS (ESI) *m/z* calculated for C<sub>23</sub>H<sub>14</sub>O [M]<sup>+</sup>: 306.1045, found: 306.1037.

2BP (yield = 9.4%) M.p. 164–167 °C. <sup>1</sup>H NMR [500 MHz, DMSO(*d*<sub>6</sub>),  $\delta$ ]: 8.50 (d, *J* = 7.7, 2H), 8.43 (d, *J* = 9.3 Hz, 2H), 8.32 (d, *J* = 9.2 Hz, 2H), 8.25 (t, *J* = 7.7 Hz, 1H), 8.13 (s, 1H), 7.88 (d, *J* = 8.2, 4H), 7.71 (t, *J* = 7.5, 2H), 7.57 (t, *J* = 7.8, 4H). <sup>13</sup>C NMR [125 MHz, DMSO(*d*<sub>6</sub>),  $\delta$ ]: 201.94, 131.41, 131.21, 130.37, 129.87, 128.03, 127.43, 127.20, 124.39, 124.18, 123.19, 30.71. IR (KBr, cm<sup>-1</sup>): 3053, 1656, 1585, 1516, 1446. Elemental analysis: calcd. value for C<sub>30</sub>H<sub>18</sub>O<sub>2</sub>: 87.78% C, 4.42% H; found: 87.63% C, 4.61% H. HRMS (ESI) *m/z* calculated for C<sub>30</sub>H<sub>18</sub>O<sub>2</sub> [M]<sup>+</sup>: 410.1307, found: 410.1305.

2'BP (yield = 9.6%) M.p. 233–238 °C. <sup>1</sup>H NMR [500 MHz, DMSO(*d*<sub>6</sub>),  $\delta$ ]: 8.38 (d, *J* = 8 Hz, 2H), 8.25 (d, *J* = 9.5 Hz, 2H), 8.18 (d, *J* = 9.5 Hz, 2H), 8.10 (d, *J* = 7.5 Hz, 2H), 7.73 (d, *J* = 7.7 Hz, 4 H), 7.64 (t, *J* = 7.1, 2H), 7.49 (t, *J* = 7.7, 4H). <sup>13</sup>C NMR [125 MHz, DMSO(*d*<sub>6</sub>),  $\delta$ ]: 202.20, 133.33, 132.31, 129.07, 128.20, 127.73, 126.39, 125.35, 123.73, 30.64. IR (KBr, cm<sup>-1</sup>): 3051, 1649, 1571, 1490, 1442. Elemental analysis: calcd. value for C<sub>30</sub>H<sub>18</sub>O<sub>2</sub>: 87.78% C, 4.42% H; found: 87.71% C, 4.69% H. HRMS (ESI) *m/z* calculated for C<sub>30</sub>H<sub>18</sub>O<sub>2</sub> [M]<sup>+</sup>: 410.1307, found: 410.1301.

2''BP (yield = 37.5%) M.p. 155–158 °C. <sup>1</sup>H NMR [500 MHz, DMSO(*d*<sub>6</sub>),  $\delta$ ]: 8.42 (d, *J* = 7.5 Hz, 2H), 8.35 (s, 2H), 8.11 = (d, *J* = 3 Hz, 2H), 8.09 (s, 2H), 7.71 (d, *J* = 8.25, 4H), 7.61 (t, *J* = 8.5, 2H), 7.47 (t, *J* = 7.25, 4H). <sup>13</sup>C NMR [125 MHz, DMSO(*d*<sub>6</sub>),  $\delta$ ]: 197.82, 138.27, 134.29, 134.25, 132.99, 130.63, 129.43, 129.36, 128.57, 127.54, 126.14, 125.97, 126.14, 124.22. IR (KBr, cm<sup>-1</sup>): 3051, 1654, 1595, 1446, 1446. Elemental analysis: calcd. value for C<sub>30</sub>H<sub>18</sub>O<sub>2</sub>: 87.78% C, 4.42% H; found: 87.68% C, 4.59% H. HRMS (ESI) *m/z* calculated for C<sub>30</sub>H<sub>18</sub>O<sub>2</sub> [M]<sup>+</sup>: 410.1307, found: 410.1298.

3BP (yield = 18.9%) M.p. 183–187 °C. <sup>1</sup>H NMR [500 MHz, DMSO(*d*<sub>6</sub>),  $\delta$ ]: 8.63 (d, *J* = 9.7 Hz, 1H), 8.54 (d, *J* = 9.3 Hz, 1H), 8.42 (d, *J* = 9.2 Hz, 1H), 8.35 (s, 2H), 8.30 (d, *J* = 7.8 Hz, 1H), 8.23 (s, 1H), 8.89 (m, 4H), 7.85 (d, *J* = 7.7 Hz, 2H), 7.75 (m, 3H), 7.63 (m, 6H). <sup>13</sup>C NMR [125 MHz, DMSO(*d*<sub>6</sub>),  $\delta$ ]: 197.18, 196.63, 196.52, 137.60, 137.48, 137.43, 135, 133.93, 133.90, 132.89, 132.65, 131.81, 130.42, 130.27, 130.26, 130.17, 129.77, 128.90, 128.88, 128.85, 128.06, 127.34, 127.22, 127.17, 126.44, 125.50, 124.50, 124.15, 123.64. IR (KBr, cm<sup>-1</sup>): 3055, 1654, 1593, 1568, 1446. Elemental analysis: calcd. value for C<sub>37</sub>H<sub>22</sub>O<sub>3</sub>: 86.36% C, 4.31% H; found: 87.41% C, 4.45% H. HRMS (ESI) *m/z* calculated for C<sub>37</sub>H<sub>22</sub>O<sub>3</sub> [M]<sup>+</sup>: 514.1569, found: 516.1552.

4BP (yield = 1.9%) M.p. 283–285 °C. <sup>1</sup>H NMR [500 MHz, DMSO(*d*<sub>6</sub>),  $\delta$ ]: 8.33 (s, 4H), 8.20 (s, 2H), 7.81 (d, *J* = 9.25 Hz, 8H), 7.65 (t, *J* = 7.85 Hz, 4H), 7.50 (t, *J* = 7.85 Hz, 8H). <sup>13</sup>C NMR [125 MHz, DMSO(*d*<sub>6</sub>),  $\delta$ ]: 196.93, 137.82, 134.56, 134.39, 130.80, 130.19, 129.41, 127.75, 127.46, 124.62. IR (KBr, cm<sup>-1</sup>): 3055, 1654, 1593, 1568, 1446. Elemental analysis: calcd. value for C<sub>44</sub>H<sub>26</sub>O<sub>4</sub>: 85.42% C, 4.24% H; found: 85.63% C, 4.31% H. HRMS (ESI) *m/z* calculated for C<sub>44</sub>H<sub>26</sub>O<sub>4</sub> [M]<sup>+</sup>: 618.1831 found: 618.1820.

### 3. Results and discussion

Adding a stoichiometric quantity of benzoyl chloride to a solution of pyrene (P) and  $\text{AlCl}_3$  in carbon disulfide ( $\text{CS}_2$ ) at ambient temperature gave the benzoyl derivatives (1–4BP) in low to moderate yields (Scheme S1; ESI†). Though Harvey and co-workers<sup>19</sup> reported 1BP, 2BP and 2''BP, the synthesis of 2''BP, 3BP and 4BP is yet to be explored. Single-crystal X-ray analyses (SCXRD) of 1–4BP were not reported earlier. SCXRD analyses were performed on  $0.20 \times 0.20 \times 0.15$  mm crystalline samples obtained through slow evaporation of 1–4BP from varying compositions of chloroform:acetone mixtures (Table S1; ESI†). Benzoyl derivatives 1BP ( $P\bar{1}$ ), 2BP ( $P\bar{1}$ ) and 3BP ( $P\bar{1}$ ) display solvent-free triclinic crystal systems, while 2''BP ( $P2_1/n$ ), 2''BP ( $C2/c$ ) and 4BP ( $P2_1/n$ ) exhibit solvent-free monoclinic crystal systems (Scheme 1, row III, Table S2; ESI†).

Frontier molecular orbital (FMO) analysis, cyclic voltammetry, UV-vis absorption and emission measurements were employed to investigate the extent of perturbations in pyrene imparted by incremental benzoyl groups. FMO analyses of 1–4BP show that the electron density of HOMO (Fig. 1a) is distributed in pyrene units, while the electron density of LUMO is mostly localized on the pyrene chromophore with a moderate extension to the carbonyl group(s). The low-lying excited electronic states mainly result from well-described  $\pi$ - $\pi^*$  transitions with a minor contribution from the  $n$ - $\pi^*$  character. The decrease in the HOMO–LUMO gap from 3.59 eV (1BP) to 3.18 eV (4BP) is attributed to the increase in the effective conjugation due to the carbonyl groups on the pyrene unit (Table S3; ESI†). Cyclic voltammetry (0.1 M  $n\text{Bu}_4\text{NPF}_6$  in acetonitrile) of 1BP (Fig. 1b) exhibits an oxidation peak at 1.47 V, while the reduction peak appears at  $-1.50$  V. The decrease in the HOMO–LUMO gap of

benzoylpyrenes (2.97 eV for 1BP; 2.61 eV for 4BP; Table S3; ESI†) in comparison with P (3.37 eV) is in agreement with the FMO analysis.<sup>20</sup>

The steady state absorption spectra of 1–4BP in chloroform exhibit two distinct bands: a band centered around 250–300 nm and another around 300–425 nm (Fig. 1c). Time-dependent density functional theory (TDDFT)<sup>21</sup> calculations suggest that the observed bands are a combination of several electronic transitions (Table S4; ESI†) with the longer wavelength band due to the  $\pi$ - $\pi^*$  transition. The  $\lambda_{\text{max}}$  of long-wavelength transition of 1BP in chloroform is red-shifted by 12 nm compared to P. 2–4BP display remarkable red-shift in the long-wavelength region, which could be attributed to the increase in the number of benzoyl group(s). Upon excitation at 380 nm, 1BP in chloroform exhibits an emission band centered at around 450 nm (Fig. S2a, Table S5; ESI†). The emission maximum is *ca.* 50 nm red-shifted in comparison with P under similar conditions. However, even after a further increase in the number of benzoyl groups, the emission maximum remains unchanged (*ca.* 450 nm). A very low fluorescence quantum yield was observed for 1–4BP ( $\Phi_{\text{Fl}} \leq 1.0\%$ , Table S5; ESI†) in chloroform when compared to P ( $\Phi_{\text{Fl}} = 65\%$ ).<sup>22</sup>

Picosecond time-resolved fluorescence measurements of 1–4BP indicate very short lifetimes ( $<100$  ps pulse width at  $\lambda_{\text{ex}} = 375$  nm) when monitored at respective emission maxima (Fig. S2b; ESI†). In order to rule out the possibility of aggregation of 1–4BP in chloroform (0.1–1  $\mu\text{M}$ ), we monitored the lifetime at the far red shifted emission. Time-resolved measurement at the longer emission wavelength exhibited a very short lifetime ( $<100$  ps pulse width at  $\lambda_{\text{ex}} = 375$  nm) similar to that observed at the respective emission maxima. An obvious shoulder peak at around 550 nm was observed in the emission spectrum of 2''BP. Wavelength dependent time-resolved fluorescence and excitation spectra invalidate any possibility of aggregation of 2''BP in solution under these conditions.

As stated above, low  $\Phi_{\text{Fl}}$  for 1–4BP could result from an efficient intersystem crossing (ISC) induced by strong mixing of nearly-degenerate singlet and triplet states (Fig. 1d, Table S5; ESI†). The ISC efficiency of 1–4BP was investigated by employing nanosecond time-resolved absorption spectroscopy (Fig. S3, Table S5; ESI†). Upon excitation at 355 nm, 1BP exhibits absorption maximum at 520 nm corresponding to the triplet–triplet transition of pyrene<sup>24</sup> having a lifetime of 2.1  $\mu\text{s}$ . Similar features for triplet–triplet absorption were also observed for 2–4BP (Table S5; ESI†). Estimation of the triplet quantum yield ( $\Phi_{\text{T}}$ ) of 1BP based on triplet–triplet energy-transfer to  $\beta$ -carotene<sup>20</sup> shows a value of 48% (Fig. S4, Table S5; ESI†). We observed that  $\Phi_{\text{T}}$  decreases with an increase in the number of benzoyl groups (Table S5; ESI†). Time-gated emission measurements of 1–4BP in ethanol at 77 K show extremely weak phosphorescence when excited at 380 nm (Fig. S2c, Table S5; ESI†). With an increase in the number of benzoyl groups, systematic red-shift from 510 to 634 nm in the phosphorescence emission maximum was observed. In addition, non-radiative pathways could also operate to cause a significantly reduced fluorescence quantum

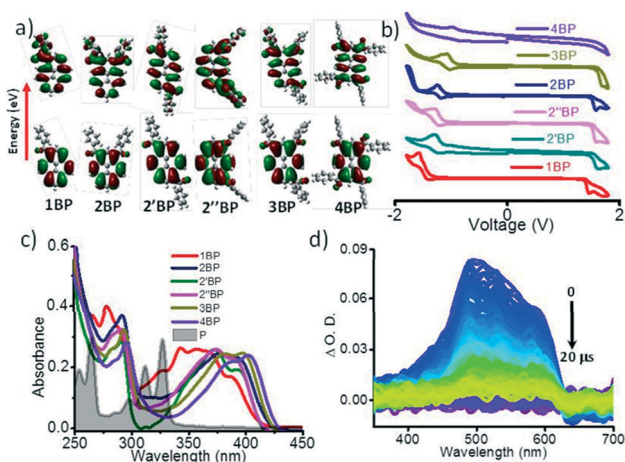


**Fig. 1** a) Frontier molecular orbital (FMO) analysis of 1–4BP calculated from the B3LYP/6-311G\*\*+ level of theory. Lower and upper plots represent the HOMOs and LUMOs, respectively. b) Cyclic voltammograms of 1–4BP in acetonitrile. c) Absorption spectra of 1–4BP; the area filled spectrum (grey) represents the absorption spectrum of pyrene.<sup>23</sup> d) Nanosecond transient absorption spectrum of 4BP in chloroform.

yield of 4BP in chloroform when compared to P. Bond rotations from benzoyl functional groups can contribute to energy dissipative pathways.

Having established the photophysical properties of 1–4BP in solution, further efforts were made to correlate the optical properties in the crystalline state. Detailed analyses of the single-crystal X-ray structures decipher the role of terminal benzoyl groups in impeding the pyrene–pyrene nearest-neighbour interactions in crystalline 1–4BP. Single-crystal X-ray analysis of 1BP shows an interplanar distance ( $\pi$ – $\pi$ ) of 3.50 Å between the two nearest pyrene units having a transverse slip (along the molecular short axis of the pyrene unit) of 0.69 Å and a longitudinal slip (along the molecular long axis of the pyrene unit) of 0.93 Å. The observed transverse/longitudinal displacement complements the phenyl rings to adopt an end-to-face ( $\text{CH}\cdots\pi \sim 2.9$  Å) interaction with the  $\pi$ -electron cloud of the neighbouring pyrene unit. With the increase in the number of benzoyl groups in 2–4BP, a progressive rise in the steric contribution causes an increase in the transverse/longitudinal displacement of the vicinal pyrene units in the crystal structure (Fig. S5 & S6, Table S6; ESI†). In 4BP, the bulky benzoyl group hampers the strong aggregation, inducing a transverse shift (5.65 Å), prohibiting any  $\pi$ -contacts between neighbouring pyrene units. The longitudinal and transverse offset imparts different degrees of orbital overlap between the pyrene units that are separated at their van der Waals distances (*ca.* 3.35–3.59 Å) in crystalline 1–4BP (Scheme 1, row II, Table S6; ESI†). This intermolecular offset of the vicinal pyrene units reduces the  $\pi$ – $\pi$  interaction that is attributed to the observed decrease in the orbital overlap from 45.92% (1BP) to 0.95% (4BP) (see the ESI†). Interplanar C–H $\cdots$ O contacts<sup>26</sup> support the pyrene units for an extended interaction along all axes in the crystalline arrangement of 1–4BP (Fig. S7; ESI†).

Intrigued by the sterically controlled longitudinal/transverse shift of the intermolecular vicinal pyrene units, further efforts were made to explore the photophysical properties of crystalline 1–4BP. Diverse colours in the crystalline 1–4BP ranging from pale yellow – yellow – orange red (Scheme 1, row III) were observed due to the intermolecular offset of the vicinal pyrene units in the crystalline state. The diffuse reflec-

tance absorption spectra of crystalline 1–4BP exhibit a broad band centered around 350–450 nm, with an additional absorption tail extending to 500 nm in 1BP (Fig. 2a, Table S5; ESI†). The presence of benzoyl group(s) results in a red-shift in UV-vis absorption, for example 114 nm (1BP) and 60 nm (4BP), when compared to crystalline P. Upon excitation at 380 nm, crystalline 1BP exhibits a broad emission band with the maximum centered at 620 nm red-shifted by 148 nm compared to crystalline P. A systematic blue-shift in the emission maximum was observed upon further increase in the number of benzoyl groups, when compared to crystalline 1BP (Scheme 1, row III and Fig. 2b & S8, Table S5; ESI†). In spite of the significant  $\pi$ -overlap ( $\pi$ – $\pi$ ; 39.91%) in crystalline P, a blue-shift in the emission wavelength was observed when compared to crystalline 1–4BP. A marked increase in the separation ( $d_{\pi-\pi} \sim 3.53$  Å) between the molecular planes of vicinal pyrene units in crystalline P (Table S6; ESI†) when compared to the crystalline BP derivatives could cause the blue-shift in the emission spectrum. The observed differences in the emission maxima for crystalline 1–4BP could be a combined consequence of different i) degrees of  $\pi$ – $\pi$  overlap and ii) distances between the molecular planes of the adjacent pyrene units. However, contributions from the non-nearest neighbour can also contribute to the overall electronic coupling that can influence the peak positions in the emission spectra. Significant red-shift in the emission wavelength dependent excitation spectra compared to the corresponding steady-state absorption spectra of crystalline 1–4BP suggests the possible ground state interaction between the vicinal pyrene units (Fig. S9; ESI†).<sup>27</sup> The substantially red-shifted dimer/excimer-like emission of 1BP could arise from the significant orbital overlap ( $\pi$ – $\pi$ ; 45.92%) between the nearest pyrene units. The nearly slipped out ( $\pi$ – $\pi$ ; 0.95%) pyrene–pyrene stack along the molecular long axis in 4BP results in a monomer-like emission possessing vibronic features.

Upon excitation at 375 nm, picosecond time-resolved fluorescence measurements of crystalline 1BP show tri-exponential decay having lifetimes of 2.5 ns (82%), 8.5 ns (12%) and 0.7 ns (6%), when monitored at 620 nm (Fig. S10, Table S5; ESI†). The long fluorescence lifetime in crystalline 1BP when compared to that in solution (<100 ps) could arise

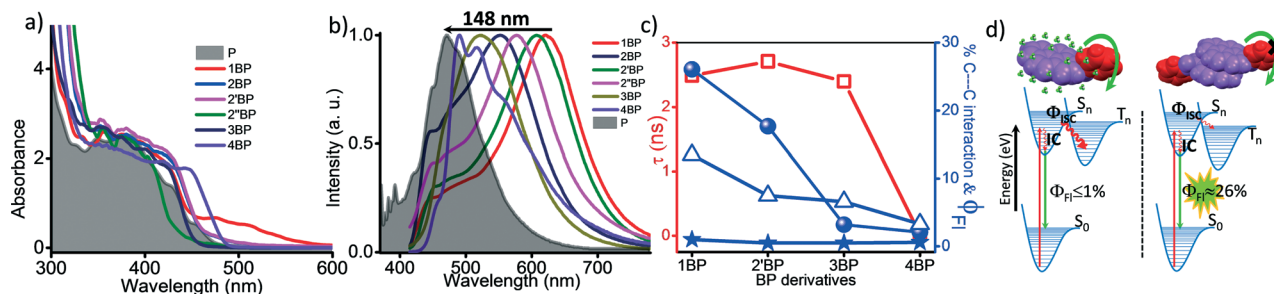


Fig. 2 a) Absorption; b) fluorescence spectra of crystalline 1–4BP derivatives;  $\lambda_{\text{exc}} = 380$  nm; the area filled spectrum (grey) represents the absorption and emission spectra of crystalline pyrene;<sup>25</sup> c) indicates  $\tau_{\text{Fl}}$  (major component;  $\square$ );  $\Phi_{\text{Fl}}$  ( $\bullet$ ) of 1–4BP in the crystalline state;  $\Phi_{\text{Fl}}$  ( $\star$ ) of 1–4BP in solution and %C–C interaction ( $\pi$ – $\pi$ ;  $\Delta$ ) obtained from Hirshfeld analysis<sup>17</sup> (Table S7; ESI†) and d) the Jablonski diagram depicting energy levels in solution (monomeric) and aggregated (crystalline) state in 1BP.

from excimer/ground state aggregation of neighbouring pyrene units possessing different orbital overlaps in the crystalline state. Similarly, crystalline 2–4BP show a tri-exponential fluorescence emission profile with a remarkable decrease in the lifetime of the corresponding major component (Fig. 2c, Table S5; ESI†). A radiative decay rate constant ( $k_r$ ) of  $1.56 \times 10^8 \text{ s}^{-1}$  and  $0.59 \times 10^8 \text{ s}^{-1}$  in solution and crystalline state of 1BP, respectively, is estimated (Table S5; ESI†). The faster rate of radiative decay in solution vs. crystalline state was similarly observed in 2–3BP. The observed decrease in the rate of radiative decay in crystalline 1–3BP when compared to that in solution indicates the possibility of H-like aggregates and/or excimers of pyrene. Unusual formation of fluorescent H-aggregates was observed earlier in merocyanine dyes by Würthner and coworkers.<sup>28</sup> Notably, the small  $\pi$ - $\pi$  contact of vicinal pyrene units in 4BP imparts a monomer-like behavior in the crystalline state (Fig. 2c, Table S6; ESI†), as reported earlier.<sup>29</sup> The twisted nature of the benzoyl group(s) with respect to the plane of the pyrene chromophore drastically diminishes the aggregation of vicinal pyrene units. The observed similar rate constant in the crystalline state and solution state of 4BP confirms the monomer-like behavior in the crystalline state ( $k_r \sim 0.59 \times 10^8 \text{ s}^{-1}$ ; Table S6; ESI†).

Unravelling the processes responsible for crystallization/aggregation induced emission is vital for the design of new light emitting materials. Recent preliminary theoretical investigations have offered insights into the characteristics of induced CIE in a variety of organic/inorganic chromophores.<sup>30</sup> CIE could arise as a consequence of i) electronic (dipolar/excitonic) interactions;<sup>28,31</sup> ii) arrested vibrational/rotational motions;<sup>32</sup> and/or iii) reduced solvation<sup>33</sup> in the crystalline state. To investigate the extent of vibrationally promoted ISC in monomer vs. dimer states, the low-lying excited electronic states of 1BP and 4BP were calculated employing the TDDFT method (Fig. S11; ESI†). The energy difference between  $S_1$  and  $T_1$  states in monomeric and dimeric 1BP was found to be 1.18 and 0.94 eV, respectively. A notable lowering of the  $T_2$  energy state was also observed from monomeric (2.95 eV) vs. dimeric (2.13 eV) 1BP. Similar observations were made in monomeric vs. dimeric 4BP. Insignificant differences in energy gap between the close-lying singlet and triplet energy levels of dimeric vs. monomeric 1BP and 4BP exclude the contribution of vibrational processes in CIE. Restriction of intramolecular rotations offered to the pendent benzoyl groups in the crystalline (dimeric) state of 1–4BP may facilitate enhancement in the fluorescence, consistent with earlier reports.<sup>34</sup> Hence, CIE in 1–4BP could arise due to i) fluorescent H-like excitonic interactions; ii) arrested rotational motion of benzoyl group(s); and/or iii) lack of solvation in the crystalline state (Fig. 2d).

## 4. Conclusion

In summary, the extent of orbital overlap ( $\pi$ - $\pi$ ) between vicinal pyrene units in crystalline 1–4BP was regulated by

exploiting the steric hindrance offered *via* successive benzylation. Progressive increment in the steric hindrance causes an increase in the transverse/longitudinal displacement of the vicinal pyrene units. As a result, a 48-fold reduction in the  $\pi$ -stacking between pyrene units was observed in 4BP with respect to 1BP. Moderating the molecular stacking along with CIE through arrested intramolecular rotations of pendent benzoyl groups may give rise to green-yellow-orange solid-state emitters. Modulating the emission properties of organic crystalline materials by controlling the extent of  $\pi$ -overlap through chemical strategies could lead to the construction of high performance photo-functional materials and devices.

## Acknowledgements

M. H. acknowledges the Kerala State Council for Science, Technology and Environment (KSCSTE) for the support of this work, 007/KSYSA-RG/2014/KSCSTE. The authors thank Alex P. Andrews, IISER-TVM, for single-crystal X-ray structure analyses.

## Notes and references

- 1 T. M. Figueira-Duarte and K. Müllen, *Chem. Rev.*, 2011, **111**, 7260.
- 2 A. Laurent, *Ann. Chim. Phys.*, 1837, **66**, 136.
- 3 D. Chercka, S.-J. Yoo, M. Baumgarten, J.-J. Kim and K. Müllen, *J. Mater. Chem. C*, 2014, **2**, 9083.
- 4 T. M. Figueira-Duarte, P. G. Del Rosso, R. Trattnig, S. Sax, E. J. W. List and K. Müllen, *Adv. Mater.*, 2010, **22**, 990.
- 5 (a) X. Feng, J.-Y. Hu, F. Iwanaga, N. Seto, C. Redshaw, M. R. J. Elsegood and T. Yamato, *Org. Lett.*, 2013, **15**, 1318; (b) J. N. Moorthy, P. Natarajan, P. Venkatakrisnan, D.-F. Huang and T. J. Chow, *Org. Lett.*, 2007, **9**, 5215; (c) T. M. Figueira-Duarte, S. C. Simon, M. Wagner, S. I. Druzhinin, K. A. Zachariasse and K. Müllen, *Angew. Chem., Int. Ed.*, 2008, **47**, 10175; (d) K. C. Wu, P. J. Ku, C. S. Lin, H. T. Shih, F. I. Wu, M. J. Huang, J. J. Lin, I. C. Chen and C. H. Cheng, *Adv. Funct. Mater.*, 2008, **18**, 67; (e) X. Feng, J.-Y. Hu, L. Yi, N. Seto, Z. Tao, C. Redshaw, M. R. J. Elsegood and T. Yamato, *Chem. – Asian J.*, 2012, **7**, 2854.
- 6 (a) Q. Feng, M. Wang, B. Dong, J. He and C. Xu, *Cryst. Growth Des.*, 2013, **13**, 4418; (b) S. Varughese, *J. Mater. Chem. C*, 2014, **2**, 3499.
- 7 J. A. Foster, M. PiepenbrockMarc-Oliver, G. O. Lloyd, N. Clarke, A. K. HowardJudith and J. W. Steed, *Nat. Chem.*, 2010, **2**, 1037.
- 8 (a) Y. Sagara, T. Mutai, I. Yoshikawa and K. Araki, *J. Am. Chem. Soc.*, 2007, **129**, 1520; (b) R. Misra, T. Jadhav, B. Dhokale and S. M. Mobin, *Chem. Commun.*, 2014, **50**, 9076.
- 9 A. S. Batsanov, J. A. K. Howard, D. Albesa-Jové, J. C. Collings, Z. Liu, I. A. I. Mkhaliid, M.-H. Thibault and T. B. Marder, *Cryst. Growth Des.*, 2012, **12**, 2794.
- 10 (a) P. Sonar, M. S. Soh, Y. H. Cheng, J. T. Henssler and A. Sellinger, *Org. Lett.*, 2010, **12**, 3292; (b) K. R. J. Thomas, N.

- Kapoor, M. N. K. P. Bolisetty, J.-H. Jou, Y.-L. Chen and Y.-C. Jou, *J. Org. Chem.*, 2012, 77, 3921; (c) K. L. Chan, J. P. F. Lim, X. Yang, A. Dodabalapur, G. E. Jabbour and A. Sellinger, *Chem. Commun.*, 2012, 48, 5106.
- 11 J. B. Birks and L. G. Christophorou, *Spectrochim. Acta*, 1963, 19, 401.
- 12 S. K. Rajagopal and M. Hariharan, *Photochem. Photobiol. Sci.*, 2014, 13, 157.
- 13 (a) S. K. Rajagopal, A. M. Philip, K. Nagarajan and M. Hariharan, *Chem. Commun.*, 2014, 50, 8644; (b) R. T. Cheriya, A. R. Mallia and M. Hariharan, *Energy Environ. Sci.*, 2014, 7, 1661.
- 14 (a) R. T. Cheriya, K. Nagarajan and M. Hariharan, *J. Phys. Chem. C*, 2013, 117, 3240; (b) A. R. Mallia, R. Sathy, V. Bhat and M. Hariharan, *J. Mater. Chem. C*, 2016, 4, 2931–2935.
- 15 A. R. Mallia, P. S. Salini and M. Hariharan, *J. Am. Chem. Soc.*, 2015, 137, 15604.
- 16 K. Nagarajan, S. K. Rajagopal and M. Hariharan, *CrystEngComm*, 2014, 16, 8946.
- 17 S. K. Wolff, D. J. Grimwood, J. J. McKinnon, M. J. Turner, D. Jayatilaka and M. A. Spackman, *CrystalExplorer 3.1*, University of Western Australia, Australia, 2012.
- 18 C. F. Macrae, P. R. Edgington, P. McCabe, E. Pidcock, G. P. Shields, R. Taylor, M. Towler and J. van de Streek, *J. Appl. Crystallogr.*, 2006, 39, 453.
- 19 R. G. Harvey, J. Pataki and H. Lee, *Org. Prep. Proced. Int.*, 1984, 16, 144.
- 20 M. Hariharan, J. Joseph and D. Ramaiah, *J. Phys. Chem. B*, 2006, 110, 24678.
- 21 (a) A. D. Becke, *J. Chem. Phys.*, 1993, 98, 5648; (b) C. Lee, W. Yang and R. G. Parr, *Phys. Rev. B: Condens. Matter Mater. Phys.*, 1988, 37, 785.
- 22 T. Medinger and F. Wilkinson, *Trans. Faraday Soc.*, 1966, 62, 1785.
- 23 A. Nakajima, *Bull. Chem. Soc. Jpn.*, 1971, 44, 3272.
- 24 J. K. Thomas, J. T. Richards and G. West, *J. Phys. Chem.*, 1970, 74, 4137.
- 25 J. B. Birks and A. A. Kazzaz, *Proc. R. Soc. Lond. A Math. Phys. Sci.*, 1968, 304, 291.
- 26 H. S. Jena, *New J. Chem.*, 2014, 38, 2486.
- 27 F. D. Lewis and J.-S. Yang, *J. Phys. Chem. B*, 1997, 101, 1775.
- 28 U. Rösch, S. Yao, R. Wortmann and F. Würthner, *Angew. Chem., Int. Ed.*, 2006, 45, 7026.
- 29 Y. Sonoda, M. Goto, S. Tsuzuki and N. Tamaoki, *J. Phys. Chem. A*, 2007, 111, 13441.
- 30 (a) Q. Li and L. s. Blancafort, *Chem. Commun.*, 2013, 49, 5966; (b) X. Gao, Q. Peng, Y. Niu, D. Wang and Z. Shuai, *Phys. Chem. Chem. Phys.*, 2012, 14, 14207; (c) Y. Hong, J. W. Y. Lam and B. Z. Tang, *Chem. Commun.*, 2009, 4332.
- 31 (a) E. G. McRae and M. Kasha, *J. Chem. Phys.*, 1958, 28, 721; (b) M. Kasha, H. R. Rawls and M. A. El-Bayoumi, *Pure Appl. Chem.*, 1965, 11, 371; (c) E. E. Jelley, *Nature*, 1936, 138, 1009; (d) F. Li, N. Gao, H. Xu, W. Liu, H. Shang, W. Yang and M. Zhang, *Chem. – Eur. J.*, 2014, 20, 9991.
- 32 Z. Zhao, B. He and B. Z. Tang, *Chem. Sci.*, 2015, 6, 5347.
- 33 R. Hu, N. L. C. Leung and B. Z. Tang, *Chem. Soc. Rev.*, 2014, 43, 4494.
- 34 Y. Hong, J. W. Y. Lam and B. Z. Tang, *Chem. Soc. Rev.*, 2011, 40, 5361.